PHYSICAL REVIEW LETTERS

Vortex Lattice Transitions in Cyclic Spinor Condensates

Ryan Barnett,[1] Subroto Mukerjee,[2,3] and Joel E. Moore[2,3]

[1]*Department of Physics, California Institute of Technology, MC 114-36, Pasadena, California 91125, USA*
[2]*Department of Physics, University of California, Berkeley, California 94720, USA*
[3]*Materials Sciences Division, Lawrence Berkeley National Laboratory, Berkeley, California 94720, USA*

We study the energetics of vortices and vortex lattices produced by rotation in the cyclic phase of $F = 2$ spinor condensates. In addition to the familiar triangular lattice predicted by Tkachenko for ^{4}He, many more complex lattices appear in this system as a result of the spin degree of freedom. In particular, we predict a magnetic-field-driven transition from a triangular lattice to a honeycomb lattice. Other transitions and lattice geometries are driven at constant field by changes in the temperature-dependent ratio of charge and spin stiffnesses, including a transition through an aperiodic vortex structure. Finally, we compute the renormalization of the ratio of the spin and charge stiffnesses from thermal fluctuations using a nonlinear sigma model analysis.

One of the many remarkable properties of superfluids is the appearance of vortex lattices in rotated systems [1,2] which are analogous to the mixed state of type-II superconductors in a magnetic field. Bose condensates of atoms with nonzero integer spin [3], referred to as "spinor condensates," combine spin and superfluid ordering in different ways depending on the spin and the interatomic interaction. These condensates, and the vortices and other topological defects that they allow, have been actively studied in recent years.

Since the physics of individual defects in spinor condensates is now understood for the most experimentally relevant cases with total spin $F \leq 3$ [4,5], a natural next step is to understand the collective physics of many defects. Two examples are the vortex lattice in a rotated condensate and the superfluid transition in a two-dimensional condensate. In general, the lowest-energy vortex defects of spinor condensates have both superfluid and spin character. Although external rotation of the condensate couples only to the superfluid part, the mixed nature of the vortices means that the interaction between the spin parts is also important in determining the vortex lattice.

This Letter uses a general approach to vortex lattice phases in spinor condensates, including the Zeeman anisotropy normally present in experimental systems, to show that the cyclic phase of an $F = 2$ spinor condensate undergoes an unusual vortex lattice transition in a weak applied magnetic field. The shapes of the lattices are a result of the nontrivial spin configuration of the vortices and the interactions between them. Imaging the shape using a spin-insensitive measurement (such as time of flight) thus gives us indirect information about the spin configurations of the defects and the interactions between them. The comparison of energies of different lattices uses an Ewald summation technique (which to our knowledge has not been employed to study two-dimensional electro-

static problems) that exactly reproduces previous results obtained for simpler lattices using elliptic functions [1]. Using this method, we find several unusual possible vortex lattice structures such as the rhombic and honeycomb in addition to the familiar triangular lattice. We also show that under some conditions there is a strictly aperiodic vortex structure rather than a true lattice.

Dilute $F = 2$ bosons interact via the potential $V(|\mathbf{r}_1 - \mathbf{r}_2|) = \delta(\mathbf{r}_1 - \mathbf{r}_2)(g_0 P_0 + g_2 P_2 + g_4 P_4)$, where P_F projects into the total-spin F state and $g_F = 4\pi\hbar^2 a_F/M$ determines g_F given a_F, the scattering length in the spin-F channel. This two-body potential gives the interaction Hamiltonian [6,7]

$$\mathcal{H}_{\text{int}} = \int d\mathbf{r}: \frac{\alpha}{2}(\psi^\dagger \psi)^2 + \frac{\beta}{2}|\psi^\dagger \mathbf{F}\psi|^2 + \frac{\tau}{2}|\psi^\dagger \psi_t|^2:, \tag{1}$$

with a five-component vector field ψ whose component $\psi_m(\mathbf{r})$ destroys a boson at point $\mathbf{r}$ with $F_z = m$, $m = -2, \ldots, +2$, and $\mathbf{F}$ denoting the spin-2 representation of the $SU(2)$ generators. ψ_t is the time-reversal conjugate of ψ: $\psi_{tm} = (-1)^m \psi_m^\dagger$. Further, $\alpha = (3g_4 + 4g_2)/7$, $\beta = -(g_2 - g_4)/7$, and $\tau = \frac{1}{5}(g_0 - g_4) - \frac{2}{7}(g_2 - g_4)$. To H_{int} must be added the one-body Hamiltonian for an isotropic and spatially uniform condensate

$$\mathcal{H}_0 = \int d\mathbf{r} \frac{\hbar^2}{2M} \nabla \psi^\dagger \cdot \nabla \psi - \mu \psi^\dagger \psi, \tag{2}$$

where μ is the chemical potential. Minimizing this Hamiltonian over single-particle condensates leads to three phases: ferromagnetic, antiferromagnetic, and cyclic. The cyclic phase that will be the focus of our work occurs when $\beta, \tau > 0$ and is expected to be realized in a condensate of ^{85}Rb atoms [6]. The spinor structure of this state, having the symmetry of the tetrahedron, results in a non-Abelian homotopy group.

TABLE I. Fundamental vortices produced.

	$B < B_c$	$B > B_c$
$\frac{K_s}{K_c} > 1$	Only $(1, 0)$	Only $(1, 0)$
$1/4 < \frac{K_s}{K_c} < 1$	$(2/3, 1/3)$ & $(1/3, -1/3)$[a]	Only $(1, 0)$
$\frac{K_s}{K_c} < 1/4$	$(1/3, 2/3)$ & $(1/3, -1/3)$[b]	Only $(1, 0)$

[a]Equal numbers of $(2/3, 1/3)$ and $(1/3, -1/3)$ vortices.
[b]Twice as many $(1/3, -1/3)$ vortices as $(1/3, 2/3)$ vortices.

In all existing experiments, an important effect even at the single-particle level is the existence of anisotropy in spin space resulting from a magnetic field (B) used as part of the trapping process. Including the hyperfine interaction Γ, a Hamiltonian which reproduces the correct energies up to a constant is given by $\mathcal{H}_z = \sqrt{\Gamma^2 + (\mu_B B)^2 + \Gamma \mu_B B F_z}$, where μ_B is the Bohr magneton [8]. $\mathcal{H}$ can be expanded in powers of F_z. Since the relaxation time of the total magnetization is typically longer than the condensate lifetime, the linear term can be neglected. Particular attention has been paid to the next term which gives rise to the quadratic Zeeman effect [3]. However, due to the high symmetry of the cyclic state, this quadratic term alone is not enough to select its orientation. For this case, one therefore must consider the cubic term which is at next order.

To determine the spin states for $B \neq 0$, one must also consider the spin exchange interaction energy of the condensate per particle, which is $E_s = \frac{1}{2} n\beta \langle \mathbf{F} \rangle \cdot \langle \mathbf{F} \rangle + \frac{1}{2} n\tau |\langle \chi | \chi_t \rangle|^2$, where n is the condensate density. Since the total spin is assumed to be conserved, we can neglect the first term in this expression. Minimizing $E_s + E_z$ (where $E_z = \langle \mathcal{H}_z \rangle$) over possible spinor states, we find the following: At small magnetic fields, the spinor $\chi_{t1} = (\sqrt{1/3}, 0, 0, \sqrt{2/3}, 0)^T$ (up to any rotation about the z axis) is selected. In the classification scheme described in Ref. [9], this state is represented by a tetrahedron with one of its faces parallel to the xy plane. Upon increasing the magnetic field, there is a transition at $\mu_B B_c = n\tau/16$ to the spin orientation $\chi_{t2} = (\sin(\theta)/\sqrt{2}, 0, \cos(\theta), 0, -\sin(\theta)/\sqrt{2})^T$, where θ changes continuously with increasing magnetization. This spinor has the symmetries of a distorted tetrahedron with one of its edges parallel to the xy plane (when $\theta = \pi/4$, it has the symmetries of the regular tetrahedron). These two types of orientations are summarized in Fig. 1. The magnitude of the critical field is of the order of ambient fields in current experiments [10], but smaller fields can, in principle, be simulated by optical means [11].

An applied rotation couples to the phase of the condensate and produces point vortices in two dimensions or vortex lines in three dimensions. A vortex is a special type of configuration that is locally in an ordered state but cannot be smoothly deformed to the uniform configuration. In general, vortices form a two-dimensional lattice
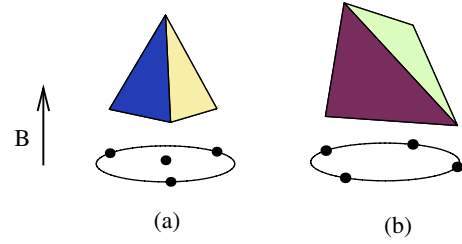

FIG. 1 (color online). Orientations of the cyclic state in an external magnetic field which breaks the spin rotational symmetry. The spin-two spinors are represented by four spin-half vectors on the unit sphere [9]. Upon increasing the magnetic field, the spinor will undergo a transition from state (a) to state (b). As indicated by the tetrahedra, orientations (a) and (b) will have rotational symmetries given by the angles $2\pi n/3$ and $2\pi n/2$, respectively (n is an integer), when rotated about the vector defined by the magnetic field. These symmetries determine what types of vortices can occur for such spin configurations.

whose properties depend on the nature of the constituent vortices and the interactions between them. For simplicity, in our study we assume that the magnetic field and the axis of rotation are in the same direction. Owing to the $2\pi/3$ spin rotation symmetry of state (a) that is stabilized at fields $B < B_c$, its vortices are of three types: (n, m), $(n - 1/3, m + 1/3)$, and $(n + 1/3, m - 1/3)$, where n and m are integers and the first argument inside the parentheses is the winding number of the phase while the second is that of the spin. Physically, this corresponds to the spinor order parameter rotating m or $m \pm 1/3$ times as the vortex is circled. The superfluid winding then has to satisfy the constraint that the wave function is single-valued. For instance, the $(2/3, 1/3)$ vortex will correspond to the spinor rotating by $2\pi/3$ counterclockwise as the vortex is circled. Only (n, m) vortices can be shown to be stable in state (b). The vortex lattices that are formed in each case have a net nonzero winding number for the phase and zero winding number for the spin.

The energetics, in addition to the above constraints on the winding numbers, depends on the stiffnesses K_c and K_s of the condensate corresponding, respectively, to the charge (phase) and the spin. The interaction energy of two vortices (x_1, y_1) and (x_2, y_2) separated by a distance r in state (a) is given by

$$E = 2\pi K_c x_1 x_2 \log(\xi/r) + \pi K_s y_1 y_2 \log(\xi/r), \quad (3)$$

where ξ is the typical radius of a vortex. $\xi = \hbar/\sqrt{2M\alpha n}$, since $\beta, \tau \ll \alpha$ in Eq. (1) for typical systems. It should be noted that K_c and K_s in Eq. (3) are not the bare stiffnesses that would be obtained from Eq. (2) but *renormalized* values due to the effects of thermal and quantum fluctuations. We will turn the issue of relating these stiffnesses to the bare values later in this Letter. We can use Eq. (3) to determine the types of fundamental vortices that are produced for different values of K_s/K_c and B. This is summarized below.

We now evaluate the energies of the lattices produced by the above fundamental vortices. Because of the long-ranged nature of the logarithmic interactions, the energy of a vortex lattice is difficult to evaluate directly. Thus, we develop a method that is similar to the Ewald summation technique for the cohesive energy of three-dimensional ionic crystals [12,13]. For simplicity, we use a scalar condensate to demonstrate the technique; the generalization to spinor condensates is straightforward and will be given presently. The energy (in units of the stiffness) of a single vortex taken to be at the origin is given by

$$\phi(0) = \sum_{\mathbf{R} \neq 0} \log\left(\frac{\xi}{\mathbf{R}}\right) - \int d^2 r \rho_0 \log\left(\frac{\xi}{r}\right), \qquad (4)$$

where $\mathbf{R}$ are the lattice vectors and ξ the size of the vortex. The second term is due to a uniform negative background charge of density ρ_0 which arises from the fact that we are working in a rotating frame of reference. Note that each of these terms diverges individually, but their difference does not. The Ewald prescription is to add and subtract a normalized Gaussian function $\frac{1}{\pi\sigma^2}e^{-r^2/\sigma^2}$ from each point charge, where σ is a screening length. For instance, the potential of a point charge at the origin screened by such a Gaussian function is $\phi(r) = \frac{1}{2}\text{Ei}(r^2/\sigma^2)$, where $\text{Ei}(x) = \int_x^\infty dt e^{-t}/t$ is the exponential integral. Proceeding along these lines, the resulting potential corresponding to Eq. (4) is

$$\phi(0) = \frac{1}{2}\sum_{\mathbf{R} \neq 0} \text{Ei}\left(\frac{R^2}{\sigma^2}\right) + \sum_{\mathbf{G} \neq 0} \rho_0 \frac{2\pi}{G^2} e^{-(\sigma^2/4)G^2}$$
$$- \log\left(\frac{\xi}{\sigma}\right) - \frac{\gamma}{2} - \rho_0 \frac{\pi}{2}\sigma^2, \qquad (5)$$

where $\mathbf{G}$ are the reciprocal lattice vectors and γ is the Euler-Mascheroni constant. The first term comes from the density of point charges screened by the Gaussian function, while second term comes from difference of the charge density of the Gaussian functions and the uniform charge density. The term $-\log(\frac{\xi}{\sigma}) - \frac{\gamma}{2}$ is obtained after subtracting off the additional Gaussian function at the origin where we omit the charge. Finally, the last term is to make the average of the screened potential zero [13]. The best check of this procedure is to see if the sum is independent of the parameter σ. The sums in real and reciprocal space in Eq. (5) converge exponentially fast. For vortices in spinor condensates, which contain windings of phase and spin, the above procedure is applied individually to each sector with the Ewald sums being weighted by the corresponding stiffnesses. The main advantage of the Ewald technique is that it can be easily generalized to treat complicated unit cells with an arbitrary number of vortices.

Let us first consider the case $B > B_c$. As noted earlier, the vortices produced by the rotation are of the type $(1, 0)$. These form the usual triangular lattice for all values of K_s/K_c. For $B < B_c$, the fractional winding numbers of the

fundamental vortices give rise to more interesting possibilities. For $1/4 < K_s/K_c < 1$, the lattice is bipartite with equal numbers of $(2/3, 1/3)$ and $(1/3, -1/3)$ vortices. We use the Ewald summation technique to numerically evaluate the energy of the lattice assuming the same parallelogram unit cell for both sublattices and an arbitrary displacement between them. We then perform a minimization of the energy over these parameters to identify the lattice that is produced at different values of K_s/K_c. The sequence of lattices is described in Fig. 2. At exactly $K_s/K_c = 1$, the two sublattices do not interact with each other, and each is a triangular lattice. As soon as K_s/K_c is lowered and the two begin to interact, the honeycomb lattice is stabilized and remains so until $K_s/K_c = 0.76$. Below this value, the vortices of one type move to the centers of the rhombic unit cells formed by the other type forming an interpenetrating rhombic lattice. The internal angle of the rhombus changes continuously with K_s/K_c from $\pi/3$ at $K_s/K_c = 0.76$ to $\pi/2$ at $K_s/K_c = 0.64$. The interpenetrating square lattice thus obtained at $K_s/K_c = 0.64$ is stable down to $K_s/K_c = 1/4$. This sequence of lattices is the same as obtained for rotating two-component condensates in the quantum Hall regime [14], or equivalently the $F = 1$ polar condensate, but the values where the transitions occur are different for $F = 2$.

For $K_s/K_c < 1/4$, a lattice with $(1/3, 2/3)$ and $(1/3, -1/3)$ vortices is obtained with twice as many of the latter as the former. Exactly at $K_s/K_c = 1/4$, the two sublattices do not interact, and each is a triangular lattice. The sublattice of the $(1/3, 2/3)$ vortices has a unit cell of length $\sqrt{2}$ times that of the $(1/3, -1/3)$ vortices. These two lattices are *incommensurate* for any rotation angle between them, which follows from showing that the nonzero
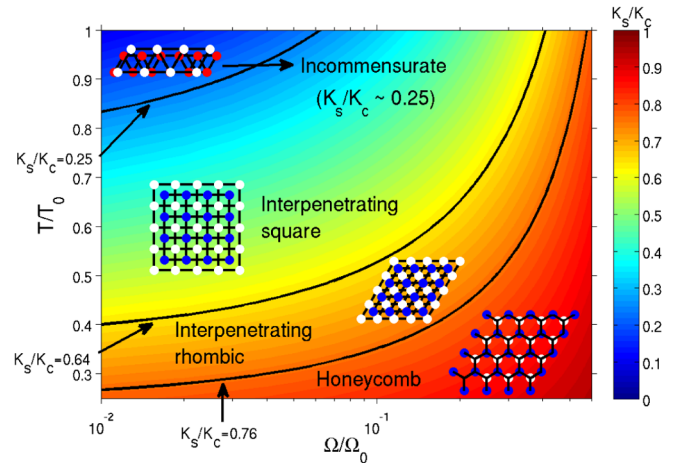

FIG. 2 (color online).   Phase diagram of the different types of vortex lattices obtained as a function of temperature and rotation rate for $B < B_c$ where $T_0 = \frac{\hbar^2 n_{3D}}{2Mk_B}\left(\frac{4\pi^4\xi^3}{3}\right)^{1/3}$ and $\Omega_0 = \frac{\pi\hbar}{M\xi^2}$. The color code for the vortices is $(2/3, 1/3)$, blue; $(1/3, -1/3)$, white; and $(1/3, -2/3)$, red. The temperature and rotation rate are related to ratio K_s/K_c via Eq. (7) for three dimensions.

squared lengths of lattice vectors in one lattice are disjoint from those in the other lattice. This incommensurability implies that the energy of interaction between the two lattices can be calculated using the Ewald technique by averaging over all displacement vectors instead of specific lattice points, and the result is zero. In the other limit, $K_s/K_c \to 0$, the interaction between all pairs of vortices is identical, and a triangular lattice is obtained. While there are several ways to distribute the two kinds of vortices in such a lattice, the lattice where the $(1/3, -1/3)$ vortices form a honeycomb lattice, while the $(1/3, 2/3)$ vortices are at the centers of each hexagon is the most symmetric one with three vortices per unit cell. The behavior between the incommensurate structure at $K_s/K_c = 1/4$ and this specific triangular structure as $K_s/K_c \to 0$ is difficult to determine reliably by our technique, since, given the existence of the incommensurate structure, there is no justification for a numerical search over unit cells with a finite number of basis vectors.

As demonstrated above, transitions between different vortex lattices can be tuned by a magnetic field B or the ratio K_s/K_c. While the field B can be applied directly or its effect simulated through optical techniques in experiments [11], the ratio K_s/K_c is more difficult to manipulate directly. In spinor condensates at close to zero temperature, this ratio is typically close to 1 but is renormalized by quantum and thermal fluctuations with the bare stiffnesses $K_s^0 = K_c^0 = \frac{\hbar^2 n}{M}$ as can be seen from Eq. (2), where n is the density of atoms. Increasing temperature (T) causes K_s and K_c to be renormalized by thermal fluctuations. To a first approximation, the renormalization at low temperature can be given by an $O(n)$ nonlinear sigma model (NLσM) with K_s corresponding to $N = 3$ and K_c to $N = 2$ [5]. The renormalization of the stiffnesses comes from the interaction between goldstone modes (spin waves) of the phase and spin at finite temperature. The nonlinear sigma model considers the interaction between these modes in a renormalization group scheme enabling us to calculate the flows of the stiffnesses. We take the stiffnesses at the short distance cutoff (ξ) to be K_s^0 and K_c^0. The flow equations for K_s and K_c are integrated up to a length scale $L = \sqrt{\pi\hbar/M\Omega}$, which is the average intervortex separation for $B < B_c$ and angular velocity Ω. We thus obtain $\frac{K_s}{K_c} = 1 - \frac{k_B T M}{2\pi\hbar^2 n_{2D}} \log(\frac{\pi\hbar}{M\Omega\xi^2})$ in two dimensions and

$$\frac{K_s}{K_c} = 1 - \frac{2Mk_BT}{\hbar^2 n_{3D}}\left(\frac{3}{4\pi^4\xi^3}\right)^{1/3}\left(1 - \sqrt{\frac{M\Omega\xi^2}{\pi\hbar}}\right) \quad (7)$$

in three dimensions. In both cases, the ratio K_s/K_c can be seen to decrease linearly with temperature from its bare value of 1. The above analysis neglected quantum effects due to Bogoliubov modes. One can on general grounds argue that they produce a weaker (T^4) dependence of

K_s/K_c at low temperature. The above analysis also assumed an unbroken spin rotation symmetry despite the presence of the magnetic field. This can be justified if the field scale is smaller than the temperature. A more rigorous analysis involves including the Zeeman term as a mass term in the NLσM and integrating the flow equation up to a length scale where this term is of order unity. If this length scale is larger than the intervortex separation, the above results would hold. If not, one would integrate from this length scale to the intervortex separation assuming an $O(2)$ model for the spin. Either way, the final renormalization of K_s/K_c would be linear in temperature with a weak B dependence in the latter case.

To conclude, we have shown using the Ewald summation technique that different types of vortex lattices can be produced in cyclic condensates as functions of magnetic field and the ratio of the charge and the spin stiffnesses. In the low-field limit, there are both abrupt transitions and continuous families of lattices as functions of the ratio of the stiffnesses, including the appearance of an incommensurate structure at one value. The ratio of the stiffnesses can, in principle, be tuned by temperature.

[1] V. Tkachenko, Sov. Phys. JETP **22**, 1282 (1966).
[2] E. J. Yarmchuk, M. J. V. Gordon, and R. E. Packard, Phys. Rev. Lett. **43**, 214 (1979).
[3] J. Stenger *et al.*, Nature (London) **396**, 345 (1998); T. L. Ho, Phys. Rev. Lett. **81**, 742 (1998); T. Ohmi and K. Machida, J. Phys. Soc. Jpn. **67**, 1822 (1998).
[4] F. Zhou, Phys. Rev. Lett. **87**, 080401 (2001); H. Mäkelä, J. Phys. A **39**, 7423 (2006); G. W. Semenoff and F. Zhou, Phys. Rev. Lett. **98**, 100401 (2007); S.-K. Yip, Phys. Rev. A **75**, 023625 (2007); R. Bar nett, A. Turner, and E. Demler, Phys. Rev. A **76**, 013605 (2007).
[5] S. Mukerjee, C. Xu, and J. E. Moore, Phys. Rev. Lett. **97**, 120406 (2006).
[6] C. V. Ciobanu, S. K. Yip, and T. L. Ho, Phys. Rev. A **61**, 033607 (2000).
[7] M. Ueda and M. Koashi, Phys. Rev. A **65**, 063602 (2002).
[8] G. Briet and I. I. Rabi, Phys. Rev. **38**, 2082 (1931).
[9] R. Barnett, A. Turner, and E. Demler, Phys. Rev. Lett. **97**, 180412 (2006).
[10] L. E. Sadler *et al.*, Nature (London) **443**, 312 (2006).
[11] F. Gerbier *et al.*, Phys. Rev. A **73**, 041602(R) (2006).
[12] P. Ewald, Ann. Phys. (Leipzig) **64**, 253 (1921).
[13] M. P. Tosi, Solid State Phys. **16**, 107 (1964).
[14] E. J. Mueller and T. L. Ho, Phys. Rev. Lett. **88**, 180403 (2002).